Quantum Simulation of Single-Qubit Thermometry Using Linear Optics

Luca Mancino,* Marco Sbroscia, Ilaria Gianani, Emanuele Roccia, and Marco Barbieri
Dipartimento di Scienze, Università degli Studi Roma Tre, Via della Vasca Navale 84, 00146 Rome, Italy
(Received 6 September 2016; revised manuscript received 7 December 2016; published 27 March 2017)

Standard thermometry employs the thermalization of a probe with the system of interest. This approach can be extended by incorporating the possibility of using the nonequilibrium states of the probe and the presence of coherence. Here, we illustrate how these concepts apply to the single-qubit thermometer introduced by Jevtic *et al.* [Phys. Rev. A **91**, 012331 (2015)] by performing a simulation of the qubit-environment interaction in a linear-optical device. We discuss the role of the coherence and how this affects the usefulness of nonequilibrium conditions. The origin of the observed behavior is traced back to how the coherence affects the propensity to thermalization. We discuss this aspect by considering the availability function.

DOI: 10.1103/PhysRevLett.118.130502

Introduction.—Thermodynamics provides a description of open systems in terms of the exchange of energy, be it in the form of either heat or work. Although it was developed first in order to give an account of such systems once they have reached equilibrium with the surrounding environment, it has recently been the object of extensions for treating transient behaviors, irreversibility, and nonequilibrium quantum processes. The knowledge gained through such exertion ranges from fundamental [1–4] to more technological issues related to nonequilibrium quantum heat machines [5–7].

Within such a context, the simplest example considers a single-particle system in contact with a thermal bath; the thermodynamic limit can still be taken, by considering a large collection of identical replicas [8]. By isolating a single element, the need of accounting for the interactions among constituents is avoided and the problem greatly simplified. The attention is then entirely devoted to the internal energy levels of this one constituent and, if this is a quantum particle, to the coherence among them. Since the presence of quantum coherence underlies the existence of distinctively quantum states, viz. the class of entangled states, it is natural to consider coherence itself as a resource, with appropriate tools for assessing and quantifying its presence [9–12].

These considerations find an immediate application in the context of thermometry, since, on the one hand, we assist at the interaction for a given time of a probe with the monitored system, while, on the other, the probe itself needs to be prepared in an informative, hence resourceful, state [13–17]. In Ref. [18], Jevtic *et al.* have discussed the implementation of an elementary thermometer with a single qubit: The task is not the estimation of arbitrary temperatures but the discrimination between two thermal baths at different temperatures. Notably, they have found that limiting the interaction time between the qubit and either bath, thus avoiding thermalization, results in an improved discrimination. This investigation opens perspectives for realizing temperature measurements at the nanoscale, when the thermometer needs to be even smaller than a nanosize thermal bath, e.g., a nanomechanical device [19] or atomic condensates [20–22].

Here, we present an experimental investigation of the results of Jevtic *et al.* with a linear-optical simulator. We show how one can determine an observable able to discriminate optimally between the two baths and how the coherence between the two energy levels of the qubit influence the performance of the thermometer. Coherence does play a role in the discrimination, but its role is not as simple as a mere enhancement; instead, it affects the time scale at which thermalization occurs. These features are well captured by the change of the availability function. Our investigations offer an experimental insight on the roles of quantum nonequilibrium states as probes for thermodynamic processes.

Qubit-bath interaction.—Our thermometer is constituted by a single qubit, governed by its Hamiltonian $\mathbb{H}_S = (\hbar\omega/2)\sigma_z$, where σ_z is the z-Pauli operator. When isolated, the two levels of the system, the excited state $|0\rangle$ and the ground state $|1\rangle$, are separated by $\hbar\omega$, which dictates the energy scale of the protocol.

The interaction of the qubit with a thermal bath, modeled as a gas of noninteracting bosons, results in either of two processes: (i) The qubit decays to the ground state transferring its energy to the thermal bath; (ii) the qubit absorbs an excitation from the reservoir, hence hopping incoherently to the excited state. The rate of the two processes is dictated by the temperature.

Since we are approaching thermodynamics as a theory describing state transformations in the presence of a thermal bath, we introduce a phenomenological model for this interaction as a quantum channel [23–26]. The corresponding map required to simulate our interaction is a generalized amplitude damping channel (GAD), that

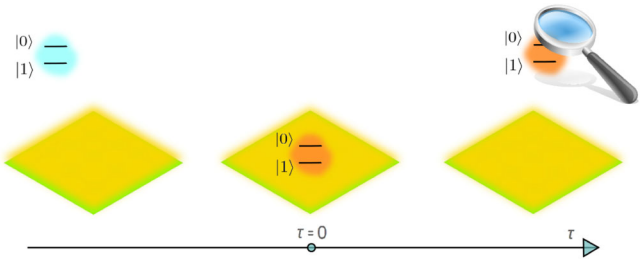

FIG. 1. Conceptual scheme of the protocol. First, the qubit is initialized in a suitable probe state, and then it is put in contact with a thermal bath of unknown temperature, either T_1 or T_2. Finally, the qubit is removed from the interaction after a time τ and measured to infer the working temperature.

utilizes two couples of Kraus operators. The first one (E_0, E_1) describes the decay process (i) via a standard amplitude damping (AD) channel [23]. The second one (E_2, E_3) reproduces the inverse process (ii); this is an AD, too, in which the roles of $|0\rangle$ and $|1\rangle$ are exchanged [27].

The GAD channel is characterized by two parameters: γ, which represents the decay rate for both the processes, and p, which is the occurrence probability of the first couple of Kraus operators; $(1-p)$ is the probability for the other couple. These two parameters are linked to the exact solution of the problem, given by the full Lindblad treatment: $(1-2\bar{N})^{-1} = (1-2p)$ and $(1-\gamma) = \exp[-(1+2\bar{N})\tau]$, where $\bar{N}$ is the average number of excitations in the bath and τ is the (dimensionless) interaction time as described in Ref. [18]. We notice that the Lindblad treatment is justified only in the Markovian limit of the dynamics [28].

Single-qubit thermometry.—Figure 1 illustrates our discrimination protocol. At $\tau = 0^-$, the thermometer is kept isolated and initialized in the state $|\psi\rangle = \cos(\theta/2)|0\rangle + \sin(\theta/2)|1\rangle$. At $\tau = 0$, the qubit is put in contact with the thermal bath, which is itself at either a "cold" temperature T_1 or a "hot" temperature $T_2 > T_1$. The different temperatures imply different occupation numbers $\bar{N}_1$ and $\bar{N}_2$; therefore, the qubit undergoes two distinct evolutions depending on the state of the reservoir. Finally, after an interaction time τ, the qubit is isolated again and then measured to determine whether the bath was cold or hot.

Full thermalization, $\tau \to \infty$, corresponds to the equilibrium regime where the qubit is in a thermal state; conventional thermometry operates within this regime. In our investigation, we extend this analysis to nonequilibrium states. The state of the qubit after the interaction with the reservoir T_i is $\rho_i(\tau)$ $(i = 1, 2)$. The protocol then aims at finding a suitable observable $\hat{\mathbb{G}}(\tau)$ allowing us to discriminate $\rho_1(\tau)$ and $\rho_2(\tau)$ optimally [29,30]. The observable $\hat{\mathbb{G}}(\tau)$ is then chosen to maximize the difference $|\mathrm{Tr}[\rho_1(\tau)\hat{\mathbb{G}}(\tau)] - \mathrm{Tr}[\rho_2(\tau)\hat{\mathbb{G}}(\tau)]|$; more details are given in Ref. [27].

Linear-optics simulation.—We illustrate these concepts by implementing a linear-optics simulator. The main advantage of using simulated dynamics is that it allows us to isolate effects stemming genuinely from the process of interest, decoupling all spurious behaviors from other unwanted interactions. The linear-optical approach has demonstrated its ability in replicating single-quantum processes even when conducted in a fully classical regime [31–36]. Indeed, this takes advantage of the fact that photons are noninteracting particles; using classical light provides a convenient way to obtain a large number of independent replicas. In this work, we adopt this approach for the simulation of an open system, where the qubit is coded in the polarization and the coupling to the reservoir occurs via the spatial mode [37,38].

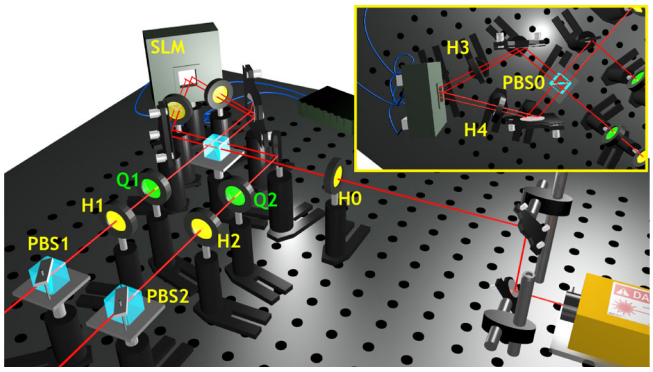

FIG. 2. Experimental linear-optical simulation. Light is provided by a diode laser emitting 680 μW at 810 nm. Its polarization is controlled by means of the H0 wave plate. The SLM, embedded in a displaced Sagnac interferometer, realizes the coupling between the polarization and path, as detailed in the text. At the two outputs, two polarization analyzers, consisting of a quarter-wave plate, a half-wave plate, and a polarizing beam splitter, are used to characterize the state after the simulated interaction. The two analysis channels 1 and 2 are kept distinct for practicality, but the results are combined for the analysis. Intensities are detected by a linear diode. Inset: Detail of the loops in the Sagnac interferometer. The presence of H3 and H4, both set at an angle of 22.5°, makes the polarization sensitive to the birefringent phase ϕ imparted by the SLM. A phase mask is applied, presenting two phase settings: In order to implement (E_0, E_1), one half on the clockwise loop is kept fixed at $\phi = 0$, while the other half is varied to simulated different interaction times. The mask is then inverted to implement (E_2, E_3).

Our experimental setup, shown in Fig. 2, consists of a displaced Sagnac interferometer where one of the mirrors is replaced by a spatial light modulator (SLM). By convention, we set the ground (excited) state $|1\rangle$ ($|0\rangle$) to be the vertical $|V\rangle$ (horizontal $|H\rangle$) polarization state. The input is initialized in a linear polarization, and then it is sent to the interferometer. The beam is then divided in two using a polarizing beam splitter (PBS0) whose outputs constitute the two arms of the Sagnac interferometer. The polarization is then coupled to the path using two half-wave plates (H3 and H4) and the SLM that imparts a birefringent phase ϕ (Fig. 2, inset) [39]. The mask displayed on the SLM makes sure that such a phase is present only on one of the arms,

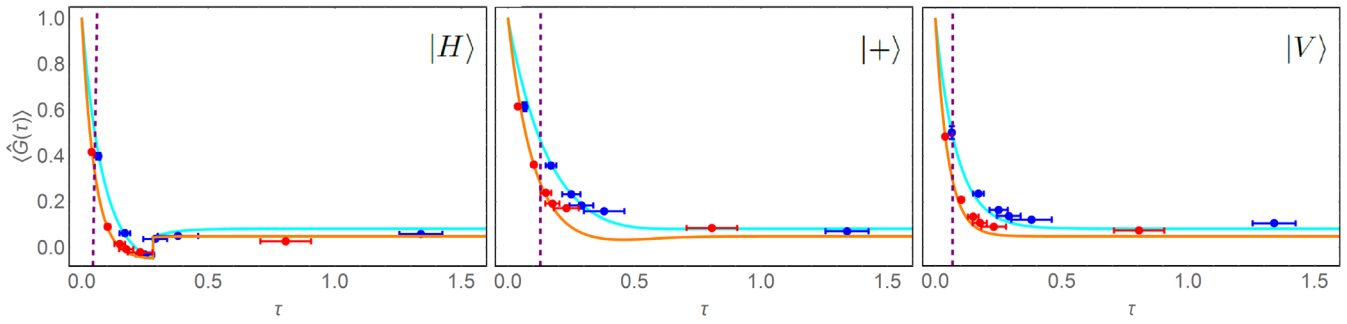

FIG. 3. Simulated temperature discrimination. The expectation values of $\hat{\mathbb{G}}(\tau)$ have been inferred from the experimentally reconstructed density matrices, corresponding to three different input states. In the three panels, red dots are for the hot bath $N_2 = 9.5$ and blue dots for the cold bath $N_1 = 5.5$; the solid lines show the predicted behavior. The vertical dashed lines indicate the optimal discrimination time, i.e., the time for which the difference of the expectation values is maximal. Vertical error bars are obtained through a Monte Carlo routine that takes into account the uncertainties on the measured intensities, while horizontal error bars reflect the uncertainties in the calibration of the SLM birefringent phase ϕ, which simulates the interaction time τ [27].

while the other arm is unaffected. Overall, this system implements the transformation $|H\rangle \to |H\rangle$ on the clockwise loop and $|V\rangle \to [\cos(\phi/2)|V\rangle + \sin(\phi/2)|H\rangle]$ on the counterclockwise loop. When the two loops are superimposed on PBS0, the horizontal component of the counterclockwise loop emerges on a separate output; this simulates the incoherent excitation of the qubit corresponding to the E_3 Kraus operator. The other output is then associated with the complementary event E_2. The damping rate is then related to the phase setting as $\gamma = \sin^2(\phi/2)$ [27]. Our device can be programed to implement the operators E_0 and E_1 by using a different phase mask on the SLM that now leaves the $|V\rangle$ component unaltered.

We reconstruct the density matrix for the qubit after its interaction with the reservoir in the following way. First, we set the interferometer in order to implement the (E_0, E_1) transformation and perform state tomography of the polarization degree of freedom [40], without distinguishing the outputs of the interferometer. We repeat the same operation, using the second setting (E_2, E_3). The two experimentally reconstructed matrices are then summed with the opportune weighting p, $(1-p)$ to obtain the state after the complete interaction [41]. We then have access to the state of the qubit at different evolution times and for both the hot and cold baths, corresponding to different choices of the phase ϕ, and of the weight p; this allows for testing the temperature discrimination procedure of the two thermal baths with different interaction times.

The results for the discrimination protocol are shown in Fig. 3, where we plot the expectation values of $\hat{\mathbb{G}}(\tau)$ for the two baths associated with three different input states: $|H\rangle$, $|+\rangle = (|H\rangle + |V\rangle)/\sqrt{2}$, and $|V\rangle$. For every simulated interaction time τ, these values are evaluated from any experimentally reconstructed density matrix ρ by obtaining the probabilities $p_+ = \langle g_+|\rho|g_+\rangle$ and $p_- = \langle g_-|\rho|g_-\rangle$, where $|g_\pm\rangle$ are the eigenvectors of $\hat{\mathbb{G}}(\tau)$ with eigenvalues ± 1; we then have that $\mathrm{Tr}[\rho\hat{\mathbb{G}}(\tau)] = p_+ - p_-$ [27].

In the three cases, the observed values follow closely the predictions and demonstrate that $\hat{\mathbb{G}}(\tau)$ serves well the purpose of discriminating between the two possible temperatures. The maximal separation occurs at short times, well before the qubit has reached full thermalization with the reservoir. These three states are associated with three different strategies: $|V\rangle$ corresponds to the ground state of the qubit; hence, we simulate the standard procedure of heating the thermometer; $|H\rangle$ corresponds to the excited state, and, hence, we simulate the cooling of the thermometer; finally, $|+\rangle$ is a coherent strategy, based on the superposition of a hot and a cold thermometer. As expected, in the steady-state regime, the use of any of the three states is equivalent, as thermalization erases any information on the initial state. Furthermore, the presence of the coherence does not help either in implementing a more effective thermometer, since the optimal separation between $\mathrm{Tr}[\rho_1(\tau)\hat{\mathbb{G}}(\tau)]$ and $\mathrm{Tr}[\rho_2(\tau)\hat{\mathbb{G}}(\tau)]$ weakly depends on the input, or a faster thermometer, as the optimal measurement time occurs at shorter times for the ground state $|V\rangle$. The main advantage of using the state $|+\rangle$ is in the possibility of maintaining a satisfactory discrimination ability for longer times, as shown by the width of the separation between the two curves; in practical applications, this eases the requirements on the controlled interaction between the qubit and the reservoir.

Availability function.—The origin of the discrimination capacity of the single-qubit thermometry has been traced back to the different trajectories of the Bloch vector associated with the qubit in the presence of either bath [18]. Such an inspection allows us to appreciate the details of the evolution that results in the observed discrimination. A complementary approach consists in considering the protocol from a purely thermodynamic perspective: Some key aspects of the evolution may show up in thermodynamic functions. The most common choice in the case of systems which interact with a reservoir of a specified temperature consists in introducing the *availability*

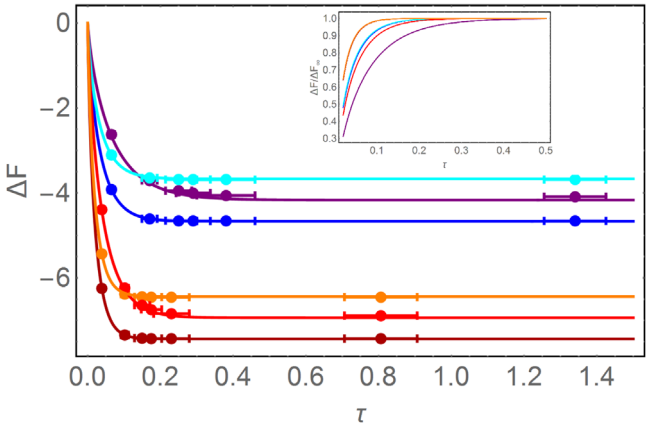

FIG. 4. Variation of the availability during the evolution of the system. The points are the free energies of the output states extracted from the experimental density matrices, using different input states: $|H\rangle$ (dark red and blue), $|D\rangle$ (red and purple), and $|V\rangle$ (orange and cyan). The solid curves are the predicted behaviors. The evolution in the presence of the hot (cold) bath results in a larger (smaller) variation of the availability. Inset: Predicted variation of the availability, normalized to its limit value ΔF_∞ at large times.

function that represents, in our case, an extension of the standard Helmholtz free energy in nonequilibrium processes with a thermal bath at a fixed temperature T; it is well established how it allows for capturing the dynamic behavior and the spontaneity of a nonequilibrium transition [42–48]. Within this framework, this thermodynamic approach may represent a valid approach for the exploration of more complex dynamics. Considering the evolution between an initial ($\rho_{\rm in}$) and final state ($\rho_{\rm out}$), the availability is defined as $\Delta F = \Delta U - T\Delta S$, where T is the temperature of the thermal bath, $\Delta U = \mathrm{Tr}[\mathbb{H}_S(\rho_{\rm in} - \rho_{\rm out})]$ is the difference of the internal energies, and ΔS is the difference in the von Neumann entropies. The latter can be evaluated as $\Delta S = -k_B \mathrm{Tr}[\rho_{\rm out}\log(\rho_{\rm out})]$, with k_B Boltzmann's constant, since $S(\rho_{\rm in}) = 0$, $\rho_{\rm in}$ being a pure state. It can be shown that the loss of availability is related to a monotonical increase of the von Neumann entropy of the system, a signature of the Markovian dynamic [49]; such a unidirectional information flow between the system and the thermal bath results in a decrease in the availability, as expected for spontaneous transformations [44,46]. The observed variation as a function of the time is shown in Fig. 4, where ΔF is measured in units of $\hbar\omega$. As expected, the variation is more pronounced when the qubit interacts with the hot bath, and there is a clear dependence of the final value on the initial state, due to the different energy variation ΔU.

Qualitative assessments on the functioning of the thermometer can be inferred by the dynamics of the variation of ΔF and how this is affected by the coherence in the initial qubit state; this not only fixes the limit value at the thermalization, but also dictates the *speed* at which this occurs. Since optimal discrimination exploits the transient states of the qubit, this constitutes a critical parameter for its performance. In the case of initialization in the coherent superposition $|+\rangle$, we are able to slow down the thermalization, and we do so in a different manner for the two possible evolutions. Therefore, we obtain a longer transient that assists the discrimination. The initialization in the two energy states $|H\rangle$ and $|V\rangle$ results in a similar, shortened time scale, as observed in the curves of Fig. 3. These behaviors are made more evident when considering the variation of the availability rescaled to the asymptotic value ΔF_∞, for all the distinct input states and reservoirs (Fig. 4, inset).

Conclusions and perspectives.—We have shown an experimental investigation of the results of Jevtic *et al.* with a linear-optical simulator. Despite the simplicity of the protocol, interesting insights are obtained on the usefulness of nonequilibrium states and the interplay with the coherence of the system. The capacity of the thermometer in distinguishing between hot and cold thermal baths strongly depends on the initial state of the qubit: While starting from the ground state might allow for a faster operation, coherence allows us to maintain a discrimination ability for longer times. The variation of the availability of the system permits us to describe such behavior invoking purely thermodynamic considerations. Within this framework, the availability of a simulation tool, which can also be applied to quantum light, may stimulate explorations to more complex dynamics. This platform could be a test bed for introducing methods of quantum metrology in thermometry [16,50] or ideas from thermometry in the monitoring of quantum channels, establishing connections between thermodynamic potentials and ultimate limits to the precision.

We are grateful to Antonella De Pasquale, Paolo Mataloni, Mauro Paternostro, and Roberto Raimondi for insightful feedback on the manuscript. We thank Fabio Sciarrino for the loan of scientific equipment. M. B. has been supported by a Rita Levi-Montalcini fellowship of MIUR.

Note added.—Recently, we became aware that similar work was being pursued by Tham *et al.* [51].

*luca.mancino@uniroma3.it

[1] C. Jarzynski, Phys. Rev. Lett. **78**, 2690 (1997).
[2] T. B. Batalhao, A. M. Souza, R. S. Sarthour, I. S. Oliveira, M. Paternostro, E. Lutz, and R. M. Serra, Phys. Rev. Lett. **115**, 190601 (2015).
[3] M. A. García-March, T. Fogarty, S. Campbell, T. Busch, and M. Paternostro, New J. Phys. **18**, 103035 (2016).
[4] N. Rach, S. Montangero, and M. Paternostro, arXiv:1605.07476.
[5] R. Alicki and D. Gelbwaser-Klimovsky, New J. Phys. **17**, 115012 (2015).
[6] M. Campisi, J. Pekola, and R. Fazio, New J. Phys. **17**, 035012 (2015).

[7] R. Uzdin, A. Levy, and R. Kosloff, Phys. Rev. X **5**, 031044 (2015).
[8] L. Szilard, Z. Phys. **53**, 840 (1929).
[9] T. Baumgratz, M. Cramer, and M. B. Plenio, Phys. Rev. Lett. **113**, 140401 (2014).
[10] D. Girolami, Phys. Rev. Lett. **113**, 170401 (2014).
[11] A. Winter and D. Yang, Phys. Rev. Lett. **116**, 120404 (2016).
[12] C. Napoli, T. R. Bromley, M. Cianciaruso, M. Piani, N. Johnston, and G. Adesso, Phys. Rev. Lett. **116**, 150502 (2016).
[13] T. M. Stace, Phys. Rev. A **82**, 011611(R) (2010).
[14] A. Monras and F. Illuminati, Phys. Rev. A **83**, 012315 (2011).
[15] M. Brunelli, S. Olivares, M. Paternostro, and M. G. A. Paris, Phys. Rev. A **86**, 012125 (2012).
[16] L. A. Correa, M. Mehboudi, G. Adesso, and A. Sanpera, Phys. Rev. Lett. **114**, 220405 (2015).
[17] L.-S. Guo, B.-M. Xu, J. Zou, and B. Shao, Phys. Rev. A **92**, 052112 (2015).
[18] S. Jevtic, D. Newman, T. Rudolph, and T. M. Stace, Phys. Rev. A **91**, 012331 (2015).
[19] M. Brunelli, S. Olivares, and M. G. A. Paris, Phys. Rev. A **84**, 032105 (2011).
[20] C. Sabín, A. White, L. Hackermuller, and I. Fuentes, Sci. Rep. **4**, 6436 (2014).
[21] T. H. Johnson, F. Cosco, M. T. Mitchison, D. Jaksch, and S. R. Clark, Phys. Rev. A **93**, 053619 (2016).
[22] M. Hohmann, F. Kindermann, T. Lausch, D. Mayer, F. Schmidt, and A. Widera, Phys. Rev. A **93**, 043607 (2016).
[23] M. Nielsen and I. L. Chuang, *Quantum Computation and Quantum Information* (Cambridge University Press, Cambridge, England, 2000).
[24] K. Fisher, R. Prevedel, R. Kaltenbaek, and K. J. Resch, New J. Phys. **14**, 033016 (2012).
[25] A. Chiuri, S. Giacomini, C. Macchiavello, and P. Mataloni, Phys. Rev. A **87**, 022333 (2013).
[26] L. T. Knoll, C. T. Schmiegelow, O. J. Farias, S. P. Walborn, and M. A. Larotonda, Phys. Rev. A **94**, 012345 (2016).
[27] See Supplemental Material at http://link.aps.org/supplemental/10.1103/PhysRevLett.118.130502 for the full theoretical treatment and additional data.
[28] H. Carmichael, *An Open Systems Approach to Quantum Optics* (Springer, New York, 1993).
[29] C. W. Helstrom, *Quantum Detection and Estimation Theory*, Mathematics in Science and Engineering Vol. 123 (Academic, New York, 1976).
[30] S. M. Barnett and S. Croke, arXiv:0810.1970.
[31] A. Schreiber, A. Gabris, P. P. Rohde, K. Laiho, M. Stefanak, V. Potocek, C. Hamilton, I. Jex, and C. Silberhorn, Science **336**, 55 (2012).
[32] A. Crespi, S. Longhi, and R. Osellame, Phys. Rev. Lett. **108**, 163601 (2012).
[33] M. Segev, Y. Silberberg, and D. N. Christodoulides, Nat. Photonics **7**, 197 (2013).
[34] T. Eichelkraut, C. Vetter, A. Perez-Leija, H. Moya-Cess, D. N. Christodoulides, and A. Szameit, Optica **1**, 268 (2014).
[35] D. N. Biggerstaff, R. Heilmann, A. A. Zecevik, M. Grärfe, M. A. Broome, A. Fedrizzi, S. Nolte, A. Szameit, A. G. White, and I. Kassal, Nat. Commun. **7**, 11282 (2016).
[36] J. Boutari, A. Feizpour, S. Barz, C. Di Franco, M. S. Kim, W. S. Kolthammer, and I. A. Walmsley, J. Opt. **18**, 094007 (2016).
[37] M. P. Almeida, F. de Melo, M. Hor-Meyll, A. Salles, S. P. Walborn, P. H. S. Ribeiro, and L. Davidovich, Science **316**, 579 (2007).
[38] A. Cuevas *et al.*, arXiv:1604.08350.
[39] G. B. Lemos, J. O. de Almeida, S. P. Walborn, P. H. Souto Ribeiro, and M. Hor-Meyll, Phys. Rev. A **89**, 042119 (2014).
[40] D. F. V. James, P. G. Kwiat, W. J. Munro, and A. G. White, Phys. Rev. A **64**, 052312 (2001).
[41] We have controlled this procedure to deliver the same results as running the matrix reconstruction algorithm on weighted data. The main advantage of our strategy consists in introducing an extra reconstruction step, serving as a further control test.
[42] L. D. Landau and E. M. Lifshitz, *Statistical Physics* (Pergamon, New York, 1980).
[43] C. Di Castro and R. Raimondi, *Statistical Mechanics and Applications in Condensed Matter* (Cambridge University Press, Cambridge, England, 2015).
[44] S. Deffner and E. Lutz, Phys. Rev. Lett. **107**, 140404 (2011).
[45] K. H. Hoffmann, B. Andresen, and P. Salamon, Phys. Rev. A **39**, 3618 (1989).
[46] M. Horodecki and J. Oppenheim, Nat. Commun. **4**, 2059 (2013).
[47] P. Skrzypczyk, A. J. Short, and S. Popescu, Nat. Commun. **5**, 4185 (2014).
[48] J. M. R. Parrondo, J. M. Horowitz, and T. Sagawa, Nat. Phys. **11**, 131 (2015).
[49] D. Chruściński and S. Maniscalco, Phys. Rev. Lett. **112**, 120404 (2014).
[50] A. De Pasquale, D. Rossini, R. Fazio, and V. Giovannetti, Nat. Commun. **7**, 12782 (2016).
[51] W. K. Tham, H. Ferretti, A. V. Sadashivan, and A. M. Steinberg, Sci. Rep. **6**, 38822 (2016).